Surface Monocrystallization of Copper Foil for Fast Growth of Large Single-Crystal Graphene under Free Molecular Flow

Huan Wang, Xiaozhi Xu, Jiayu Li, Li Lin, Luzhao Sun, Xiao Sun, Shuli Zhao, Congwei Tan, Cheng Chen, Wenhui Dang, Huaying Ren, Jincan Zhang, Bing Deng, Ai Leen Koh, Lei Liao, Ning Kang, Yulin Chen, Hongqi Xu, Feng Ding, Kaihui Liu, Hailin Peng, and Zhongfan Liu**

Commercial polycrystalline copper (Cu) foil has broad applications in CO_2 electro-reduction,[1,2] transformers,[3] batteries,[4,5] circuitry,[6,7] and other electronics industry.[8,9] In particular, Cu foil has recently become the most promising catalytic substrate for mass production of high-quality graphene films via chemical vapor deposition (CVD).[10–14] However, the commercial polycrystalline Cu foil has rough surface rich of defects, steps, and grain boundaries, which function as active sites for graphene nucleation and result in high nucleation density and random orientations.[15–18] The single-crystalline domain size of graphene is hence very limited. In addition, the domain boundaries that degrade their electrical and mechanical properties appear when misoriented domains merge together toward a continuous film. Consequently, the quality of large-scale CVD graphene films is much worse than the mechanically exfoliated counterpart. There is a big gap between conceptual and practically available graphene films for applications.[19–22]

To minimize the adverse impact of the domain boundaries, large high-quality single-crystal graphene films are highly desirable for most applications. To this end, two possible approaches involving the control over the nucleation and growth of graphene during the CVD process are proposed to achieve large high-quality single-crystal films. The first approach involves a precise control of domain orientations, enabling a seamless coalescence of adjacent domains without grain boundary defects during the epitaxial growth of graphene on a single-crystal substrate. The second approach involves the suppression of nucleation density in the graphene growth to avoid the possible formation of domain boundaries. Great efforts have recently been made along these directions, including the use of expensive single-crystal growth substrates,[23–25] the suppression of nucleation density via locally feeding carbon precursors[26] and the time-consuming pretreatments of Cu substrates (e.g., introducing oxygen, long-time annealing, melting-resolidification, smoothing, oxidative etching-assisted etc.).[27–32] As the nucleation suppression is mostly achieved by lowering the feedstock concentration during growth, the growth rate and yield in these approaches are usually very low (typically in the range of 1.8–24 μm min^{-1} and the growth time of hours to days).[27–32]

Herein, we present a practically scalable approach for surface monocrystallization of commercial Cu foils and very fast growth of large single-crystalline graphene arrays. With a simple stacking structure of Cu foils, the entire surface of polycrystalline Cu foils was readily converted into inch-sized

Dr. H. Wang, L. Lin, L. Z. Sun, X. Sun, Dr. S. L. Zhao, C. W. Tan, Dr. W. H. Dang, H. Y. Ren, J. C. Zhang, B. Deng, Dr. L. Liao, Prof. H. L. Peng, Prof. Z. F. Liu
Center for Nanochemistry
Beijing Science and Engineering Center for Nanocarbons
Beijing National Laboratory for Molecular Sciences
College of Chemistry and Molecular Engineering
Peking University
Beijing 100871, P. R. China
E-mail: hlpeng@pku.edu.cn; zfliu@pku.edu.cn

X. Z. Xu, Prof. K. H. Liu
State Key Laboratory for Mesoscopic Physics
Collaborative Innovation Center of Quantum Matter
School of Physics
Peking University
Beijing 100871, P. R. China

X. Z. Xu, J. Y. Li, L. Z. Sun, X. Sun, Dr. S. L. Zhao, C. W. Tan, H. Y. Ren, J. C. Zhang, Prof. H. L. Peng, Prof. Z. F. Liu
Academy for Advanced Interdisciplinary Studies
Peking University
Beijing 100871, China

J. Y. Li, Prof. N. Kang, Prof. H. Q. Xu
Key Laboratory for the Physics and Chemistry of Nanodevices and Department of Electronics
Peking University
Beijing 100871, P. R. China

C. Chen, Prof. Y. L. Chen
Department of Physics and Clarendon Laboratory
University of Oxford
Parks Road, Oxford OX1 3PU, UK

Dr. A. L. Koh
Stanford Nano Shared Facilities
Stanford University
Stanford, California 94305, USA

Prof. F. Ding
Institute of Textile and Clothing
Hong Kong Polytechnic University
Kowloon, Hong Kong, China

DOI: 10.1002/adma.201603579

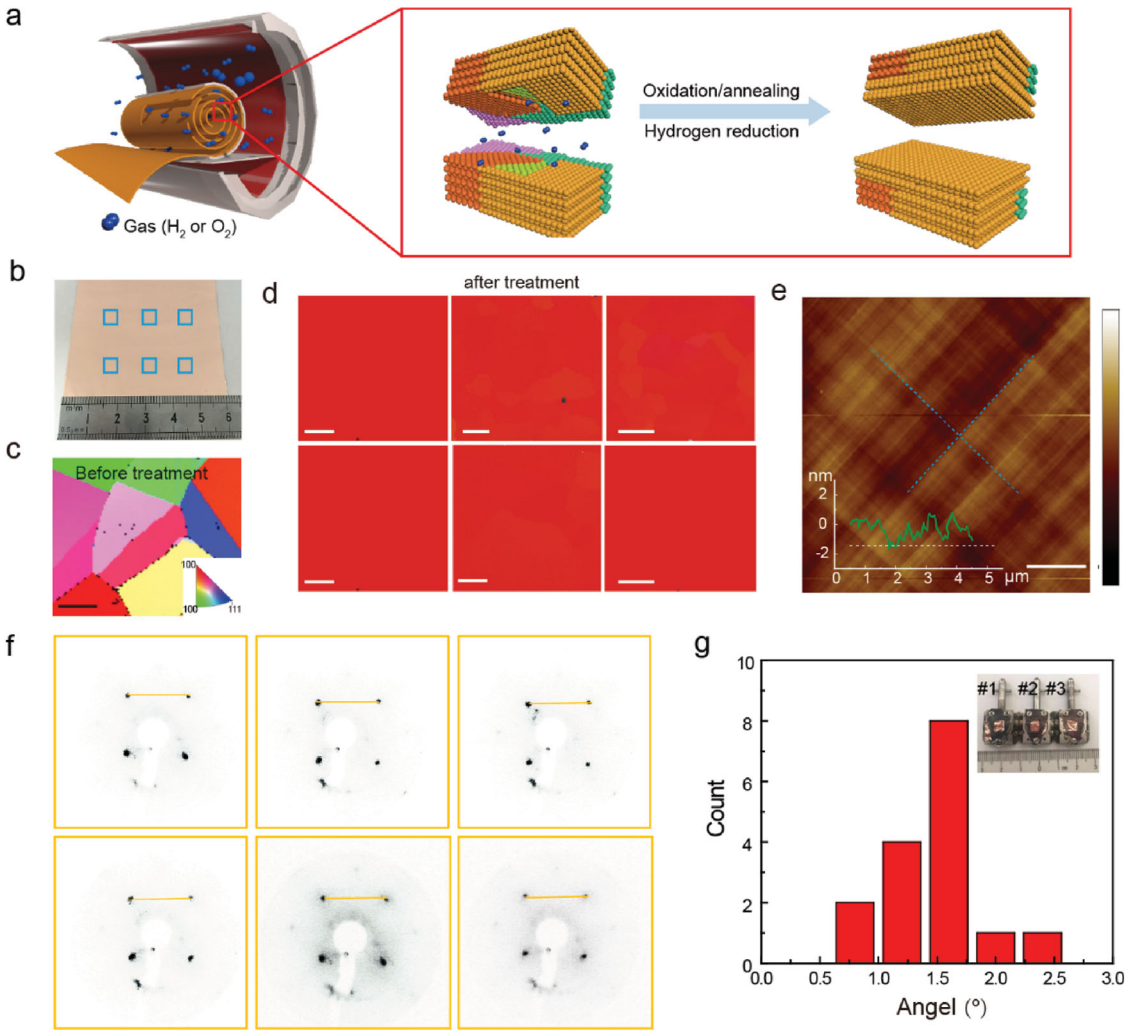

Figure 1. Surface engineering of polycrystalline Cu foil. a) Schematic illustration of the production of single-crystalline Cu (100) on the surface of polycrystalline Cu foil. b) Photograph of large-area Cu foil (6 cm × 6 cm) after surface monocrystallization. c) EBSD map of Cu foil before monocrystallization treatment. Scale bar: 50 μm. Inset: color key. d) Extensive EBSD maps taken from the specific areas marked in (b) after monocrystallization treatment. Scale bars: 50 μm. e) Typical AFM height-mode image of Cu foil in (b) after monocrystallization treatment with a z-scale of 10 nm. The blue dashed line represents the direction of Cu atomic steps. Scale bar: 2 μm. Inset: the corresponding height profile along the white dashed line in the AFM image. f) Extensive LEED patterns from one piece of Cu foil #1 (4 mm × 4 mm), six patterns were measured. g) Histogram of orientation distribution from extensive LEED patterns. Inset: Corresponding photograph of three pieces of Cu foils cut from the same large-area Cu foil (6 cm × 6 cm) placed in the sample holders.

Cu (100) single crystal via oxygen chemisorption-induced reconstruction, which enables the rapid growth of millimeter-sized single-crystalline graphene arrays under molecular flow. The maximum growth rate reaches 300 μm min^{-1}, several orders of magnitude faster than previously reported values. Our study provides an effective way to bury the giant gap between conceptual and experimentally available graphene materials for wide applications.

Figure 1a illustrates the formation process of single-crystalline Cu (100) surface on the Cu foil. Detailed methodology is described in the Experimental Section. This process relies on a stack configuration of Cu foils, in which electropolished commercial Cu foils were rolled or vertically stacked via direct physical contact with a gap of about tens of micrometers (Figure S1, Supporting Information). The surface monocrystallization of the stacked Cu foils was achieved by a high-temperature preoxidation and subsequent hydrogen reduction process in a CVD system. The evolution of on-surface microstructures and local crystallography of large-area Cu substrates have been extensively examined by electron back-scatter diffraction (EBSD), atomic force microscopy (AFM), and low-energy electron diffraction (LEED). As shown in EBSD analyses of the stacked Cu foils before and after monocrystallization treatments (Figures 1b,c,d), the entire surfaces of the stacked Cu foils exhibit a complete Cu (100) texture over a large area (6 cm × 6 cm) after the treatment (Figure 1d), indicating the formation of homogeneous Cu (100) surface on the polycrystalline Cu foil. Extensive AFM measurements (Figure 1e and Figure S2, Supporting Information) display atomically smooth surface (roughness <1.26 nm) with the atomic steps aligned in two orthogonal

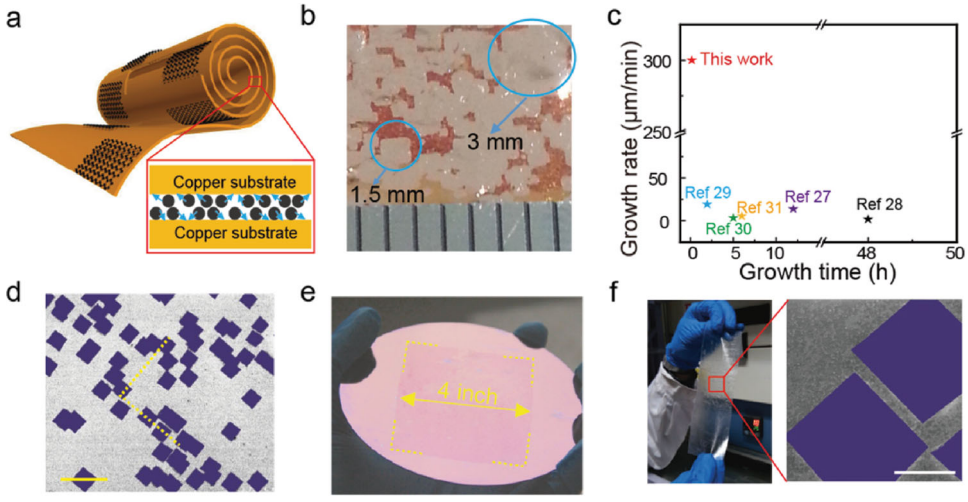

Figure 2. Fast growth of large single-crystalline graphene arrays under molecular flow. a) Schematic drawing of fast growth of single-crystalline graphene arrays under molecular flow. Inset: schematic of H_2/CH_4 transport and decomposition under molecular flow. b) Photograph of graphene domains grown on inner surface of the stacked Cu foils. c) Growth rate and growth time comparison of millimeter-sized single-crystalline graphene domains produced by different methods. d) Typical SEM image of square graphene arrays on Si/SiO_2 substrate transferred from the inner surface of the stacked Cu foil. Square graphene domains were rendered purple. The yellow dashed lines represent the directions of the edges of square graphene domain. Scale bar: 1 mm. e) Contrast enhanced photograph of the continuous graphene film transferred onto 4 inch Si/SiO_2 wafer. f) Photography of single-crystalline graphene arrays transferred onto PET substrate (left) and the corresponding SEM image (right). Square graphene domains were rendered purple. Scale bar: 100 μm.

directions, consistent with the surface structure of Cu (100) single crystal.

Representative LEED patterns of 4 mm × 4 mm Cu foil shown in Figure 1f display one set of tetragonal arrangement with identical orientations, indicating the Cu (100) structure. Furthermore, LEED characterizations were performed on additional pieces of Cu foils (inset of Figure 1g and Figure S3, Supporting Information) cut from the same large-area Cu foil (6 cm × 6 cm). Histogram of orientation distribution extracted from these extensive LEED patterns (Figure S3, Supporting Information) shows less than 1.6° rotation, justifying the single-crystalline nature of the entire centimeter-sized Cu (100). Detailed analyses and control experiments of the formation of single-crystlline Cu (100) on the surface of Cu foil were described in the Supporting Information (Figures S4–S8, Supporting Information). We believe that the formation of large-area Cu (100) single crystal originates from the reconstruction of "Cu (100)–(2 × 2)–O" on the Cu foil surface introduced by chemisorbed oxygen in the preoxidation process, in which adsorbed oxygen was subsequently removed by hydrogen reduction, thus forming the Cu (100) crystal surface.

Figure 2a presents a schematic diagram of the growth of large-domain single-crystalline graphene arrays on the stacked Cu foils. Figure 2b displays the photograph of as-grown graphene domains on the inner surface of the stacked Cu foils, among which the largest diagonal size of square domains can reach up to 3 mm within 10 min growth, indicating a significant enhancement of growth rate. The maximum growth rate of graphene domain is about 300 μm min^{-1}, which is several orders of magnitude faster than previously reported values in terms of growing millimeter-sized graphene domains on Cu foil.[27–31] Note that the whole preparation time (Figure S9, Supporting Information) of millimeter-sized graphene domains is also much shorter compared to the previously reported works involving time-consuming substrate pretreatments. The relationship between growth time and domain size is depicted in Figure S10, Supporting Information, indicating that graphene domain size strongly depends on the growth time, while the average growth rate keeps hundreds of microns per minute. Interestingly, the domain size of as-grown graphene on the inner surface of the Cu foil stack is much larger than that grown on the outer surface (Figure S11, Supporting Information), suggesting the enhancement of the growth rate is mainly caused by the special stack configuration of Cu foils.

We ascribed the fast growth of large graphene domains to a so-called molecular flow mode during the CVD process. According to the growth parameters of graphene on stacked Cu foils with a gap of 10–30 μm, the value of molecular mean-free-path (λ) of growth feedstock gas (H_2/CH_4 mixture) is calculated to be 300 μm (see the Experimental Sector and Supporting Information, Note 5). The value of Knudsen number (K_n), which is defined as the ratio of λ and scale length of the system (d), would be calculated therefore as higher than 10. This calculation indicates that the gas flow during the CVD process is under molecular flow regime (Supporting Information, Note 6).[33,34] In such gas flow regime, H_2 and CH_4 gases trapped in the narrow spaces of the stacked Cu foils can move forward with high colliding frequency toward the inner surface of opposite Cu foils, which would substantially enhance the local concentration of carbon flux and accelerate its interaction on Cu surfaces.

On the other hand, the growth of graphene on Cu surface is dominated by surface-mediated reaction under a boundary layer of active carbon species.[35] Cu foil is the catalyst for the decomposition of CH_4 and corresponding decomposition rate constant (k_s) is defined as $p*Z*e^{-Ea/RT}$, where p, Z, E_a

represents preexponential factor, collision frequency, and activation energy, respectively. Therefore, the decomposition rate is in proportion to Z. In addition, the reaction rate is $k_s \times C_s$, in which C_s is the concentration of the active carbon species at the surface. Consequently, the introduction of molecular flow can significantly reduce the thickness of the boundary layer and drastically increase the collision frequency of CH_4 and other carbon species with opposite Cu surfaces, which would altogether lead to the high yield of active carbon species. Moreover, the as-obtained carbon species are confined to the inner space of Cu stack, further increasing the concentration of active carbon species for graphene growth. In such a scenario, the growth rate of graphene would be enhanced due to the abundance of active carbon species under molecular flow regime.

Optical microscopy (OM) image of graphene square domains transferred onto 300 nm SiO_2/Si substrate confirms the uniform single-layer character of graphene film (Figure S12a, Supporting Information). By contrast, the graphene domain grown on the outer surface of the Cu foil stack under viscous flow regime (see the Supporting Information Note 6) exhibits irregular shape and numerous small multilayer islands (Figure S12b, Supporting Information). This observation indicates that the molecular flow growth mode not only accelerates the growth rate of graphene domains, but also improves the thickness uniformity. Low-magnification scanning electron microscopy (SEM) image of graphene domains transferred onto Si/SiO_2 substrate (Figure 2d and Figure S13, Supporting Information) further reveals that square graphene domain arrays aligned along the identical direction. Wafer-sized continuous graphene film can be successfully synthesized by prolonging the growth time by 20 min and transferred onto Si/SiO_2 wafer (Figure 2e). The large-scale square graphene arrays can be readily grown on a large Cu foil roll and transferred onto a transparent polyethylene terephthalate (PET) substrate (Figure 2f and Figure S14, Supporting Information), demonstrating the potential capability of our method in rapid mass production of large single-crystalline graphene arrays.

Transmission electron microscopy (TEM) was performed to examine the microstructure and crystallinity of the as-grown square graphene domains. The inset of Figure 3a displays a typical SEM image of a graphene domain transferred onto a TEM grid. Selected-area electron diffraction (SAED) patterns were collected across the entire domain. Histogram of the relative orientations of graphene lattices extracted from the extensive SAED patterns (**Figure 3**a,b and Figure S15, Supporting Information) exhibits single pronounced peaks separated by less than 0.8° rotation, justifying the single-crystalline nature of the graphene domain. Along the dashed line in the SAED patterns, the intensity of inner peaks from plane {1-100} is stronger than that of outer peaks from {1-200}, further indicating the single-layer nature.[36] Meanwhile, it could be found that two edges of as-formed square domain are of armchair geometry and the other two are of zigzag edges. Furthermore, atomic-resolution image of the as-obtained graphene domain was obtained by aberration-corrected TEM (Figure 3c), which clearly indicates perfect atomic lattices of structural defects and disorders. Raman spectra of the as-grown graphene domains (Figure S16, Supporting Information) display two characteristic G and 2D bands peaks, with a ratio of $I_{2D}/I_G > 1$ and negligible D band intensity, indicating the formation of high-quality and

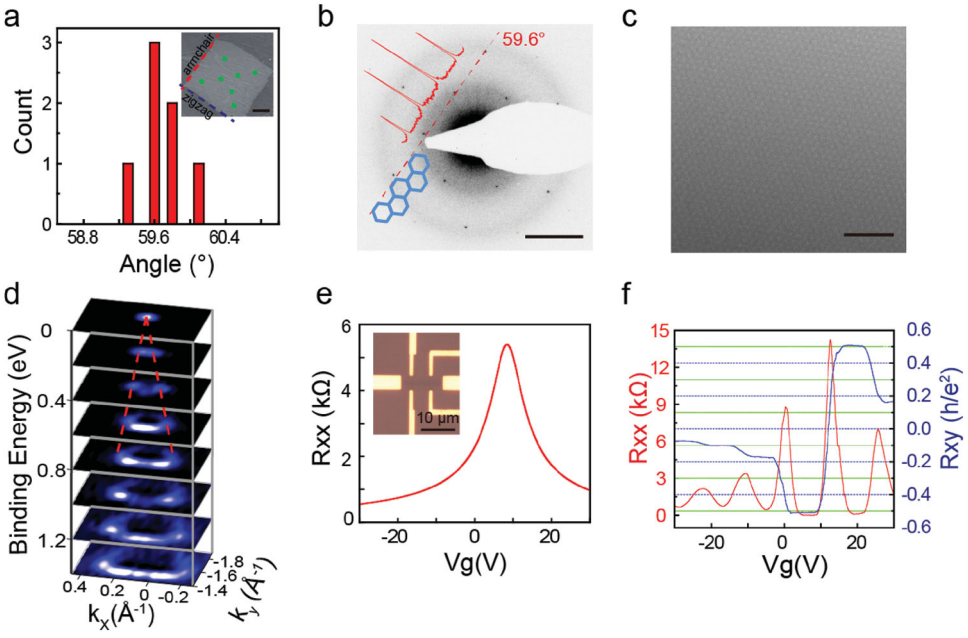

Figure 3. Structural characterization of large single-crystalline graphene domains. a) Histogram of angle distribution from extensive SAED patterns within the domain. Inset: Low-magnification SEM image of square graphene domain transferred onto TEM grid. Scale bar: 100 μm. b) Typical SAED pattern. Scale bar: 2 1/nm. Inset: intensity profile of diffraction pattern along the red dashed line. c) Atomic-resolution TEM image of the domain. Scale bar: 2 nm. d) Electronic band structure of single-crystalline graphene domain measured by micro-ARPES, in which the red dashed line indicates the profiles of Dirac cone of graphene. e) Resistance (R) versus back gate voltage (V_g) of the graphene field-effect transistor device at room temperature. Inset: the OM image of the measured standard Hall bar device. Scale bar: 10 μm. f) Longitudinal (Rxx, left) and transverse (Rxy, blue) magnetoresistances as a function of V_g at 1.9 K under a magnetic field B = 9 T.

uniform monolayer graphene.[37] Moreover, the electronic band structure of the single-crystalline graphene domain was directly measured by microspot angle-resolved photoemission spectroscopy (micro-ARPES, Figure 3d), in which a distinct Dirac cone from K point in reciprocal space and clear linear dispersion reveal the high quality of the graphene films.[38]

To evaluate the electrical properties of as-grown graphene, electrical and magneto-transport measurements were performed by fabricating standard Hall bar devices on the square single-crystalline graphene domain (inset of Figure 3e) transferred onto a highly n-doped silicon substrate with 300 nm thick silicon oxide. Resistance of the sample as a function of the back gate voltage (V_g) at room temperature (Figure 3e) demonstrates a typical ambipolar behavior. The extracted room temperature carrier mobility of this device is about 5561 $cm^2 Vs^{-1}$, comparable to the previously reported results in single-crystalline graphene on Si/SiO_2.[27–31] Moreover, the half-integer quantum Hall effect was clearly observed in a Hall bar device at 1.9 K and a magnetic field of 9 T (Figure 3f), further ascertaining the perfect electrical quality of the graphene domain.[39]

The underlying mechanism of the fast growth of large-domain single-crystalline graphene arrays on Cu surface was carefully explored. First, we studied the influence of hydrogen flow rate on the shape evolution of graphene domains. As illustrated in Figure S17a–d, Supporting Information, the shapes of graphene domains evolve from square to hexagonal and the corresponding orientations become random when the hydrogen flow rate is high. This behavior can be explained by the theoretical calculation reported previously that the graphene edges would tightly attach to the Cu surface under low hydrogen pressure, while detach from the Cu surface under high hydrogen pressure.[40] Therefore, considering the growth parameters in our method, we believe that the graphene edges are binding to the Cu (100) surface and thus the graphene growth (the orientation and shape) would be significantly influenced by the underlying Cu (100) substrate.

Secondly, we systematically investigated the orientation relationship of square graphene arrays with the underlying Cu substrate. Graphene domains grown on Cu (100) substrate are usually of tetragonal shape.[41] **Figure 4**a,b shows the low-magnification and corresponding high-magnification SEM images of the square graphene arrays grown on Cu substrate, respectively. The edges of square graphene domain are not sharp, which may arise from predominantly diffusion-limited growth mode in the rapid growth of graphene.[27] As shown in Figure 4c,d, the height- and amplitude-mode AFM images clearly identified graphene domains since the graphene coverage can induce the surface reconstruction of the underlying Cu surface.[42] The Cu (100) substrate without graphene coverage maintains parallel Cu atomic steps aligned in two orthogonal directions, consistent with that in Figure 1e and Figure S2a, Supporting Information. Remarkably, the edges of square graphene domain arrays are parallel to the atomic steps of the as-received Cu (100) substrate.

Finally, we speculate the growth process of the single-crystalline graphene arrays on Cu (100) substrates based on theoretical calculations[43,44] and our experimental data (Figure 4e). We believe that the nucleation of graphene is preferentially attached to the single-crystalline Cu (100) atomic steps aligned in two orthogonal directions, then the subsequent growth of such graphene domains would follow the direction of Cu atomic steps. Considering the square shape of graphene domains, one can conclude that the oriented alignments of Cu atomic steps on the inch-sized Cu (100) surface would lead to the uniform orientation of square graphene domain arrays on Cu (100)/polycrystalline Cu foil.

In summary, we have successfully developed an efficient strategy for the first realization of inch-sized single-crystalline

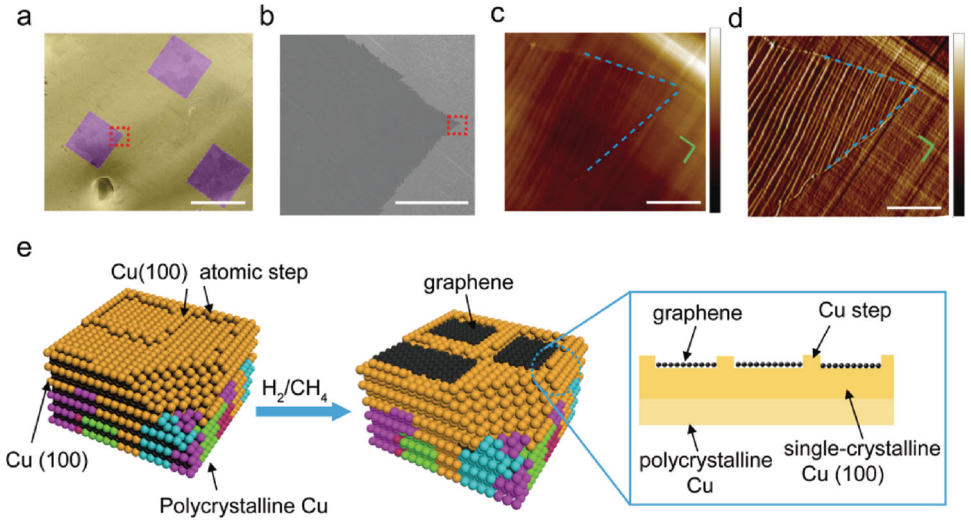

Figure 4. Growth mechanism of square graphene arrays. a) Low-magnification SEM image of graphene arrays on Cu substrate. Scale bar: 500 μm. The square graphene domains and the Cu foil were rendered purple and yellow, respectively. b) High-magnification SEM image of graphene domain marked by the dashed red box in (a). Scale bar: 100 μm. c,d) The corresponding AFM height-mode and amplitude-mode images of graphene, respectively, shown in the dashed red box in (b). Green lines represent the directions of Cu (100) atomic steps. The square graphene edges were portrayed by the dashed blue lines. Scale bars: 1 μm. e) Schematic drawing of growth mechanism of square graphene arrays. Inset: the side-view profile of graphene growth on Cu (100)/Cu foil.

Cu (100) surface on stacked polycrystalline Cu foil. Large-scale square arrays of millimeter-sized single-crystalline graphene were readily achieved on the as-obtained Cu (100) surface with a record growth rate of 300 μm min^{-1} under a molecular flow growth mode. With a practical scalability, we anticipate our present work to be a prospective point for the surface monocrystallization of commercial polycrystalline Cu foil at an industrial scale, which not only provides a high-quality substrate for graphene growth, but also offers a kind of potential electrocatalyst for CO_2 reduction with a high selectivity and efficiency. More importantly, our energy-efficient and time-saving synthetic method to large-sized graphene single crystals may present a significant step toward the real industrial application of high-quality graphene.

Experimental Section

Surface Monocrystallization of Cu Foil: Commercially available Cu foil (98% purity, 25 μm thick, Alfa Aesar #46365) was first electrochemically polished in electrolyte solution composed of phosphoric acid and ethylene glycol (V/V = 3:1) with a bias of 2 V for 30 min. The single-crystalline graphene growth was carried out in a homemade low-pressure CVD system. Stacked or rolled-up Cu foils were placed in the hot center of the furnace (Lindberg/Blue M) equipped with a 1 inch diameter quartz tube and the system was pumped to a base pressure of 1 Pa. For the stacked Cu foils, the two separate sheets just sat on top of each other. Then the Cu foil stack or foil roll was heated up to 1035 °C without additional gas while maintaining the initial pressure of 1 Pa. After reaching 1035 °C, the Cu foil continued to be annealed for 0.5–1 h. Then 100–300 sccm hydrogen, corresponding to a pressure of about 150–500 Pa, was introduced for 10–15 min to remove the adsorbed oxygen of Cu foil surface.

Growth of Single-Crystal Graphene: The graphene growth on the pretreated Cu foil after surface monocrystallization was initiated by introducing 0.5–3 sccm methane and maintained for 5–20 min according to the request of target samples. Finally, the system was rapidly cooled down to room temperature by pulling the sample out from the high-temperature zone to room temperature without changing the gas flow.

Graphene Transfer: Graphene grown on Cu foil was transferred onto the target substrate with the assistance of polymethyl methacrylate (PMMA). The sample was floated in sodium persulfate solution for 30 min to etch the Cu foil. Subsequently, PMMA was removed by hot acetone vapor after graphene/PMMA film was loaded onto SiO_2/Si or TEM grid. Specifically, the graphene was transferred to the PET substrate according to a hot lamination and electrochemical delamination methods.[14]

Characterizations: EBSD measurements were carried out on AJEOLJSM-6500F operated at 10 kV voltage. The step size was 2 μm. LEED was performed on Omicron LEED system in ultrahigh vacuum (UHV) with base pressure below 3×10^{-7} Pa. Specifically, we cut three pieces of Cu foil with a size 4 mm × 4 mm while keeping the edge direction of Cu foil unchanged along the diagonal direction of the 6 cm × 6 cm Cu foil with a space of about 1.5 cm. Auger electron spectroscopy (AES) was performed on Riber MAC 2 system in UHV with base pressure below 3×10^{-7} Pa. AFM was carried out on a Bruker Dimension Icon using the tapping mode. The OM and SEM images were obtained on an Olympus BX51 optical microscope and a Hitachi S4800 field-emission scanning electron microscope, respectively. Raman spectrum was collected on a Horiba HR800 Raman system with 514 nm laser wavelength. TEM imaging and corresponding SAED were performed using a FEI Tecnai F20 TEM operated at 200 kV. Aberration-corrected, high-resolution TEM imaging was performed using a FEI 80–300 Titan operated at 80 kV. The instrument was equipped with a spherical aberration corrector in the image-forming (objective) lens and a monochromator. The amorphous carbon-covered and lacey carbon film supported on copper grids were used for SAED and aberration-corrected TEM characterization, respectively. Micro-ARPES measurement was conducted on the Spectromicroscopy beamline 3.2 L at Elettra Synchrotron Light Source utilizing 74 eV light with a spot size smaller than 0.8 um at 110 K. The overall energy, angle, and lateral resolution were 30 meV, 1°, and smaller than 1 um, respectively.

Device Fabrication and Transport Measurements: Electron beam lithography (EBL) (Raith 150 2nd) and reactive ion etching O_2 etching (Trion technology minilock III) were used to pattern graphene. After that, EBL and electron-beam evaporation (Kurte J. Lesker AXXIS) were employed to pattern the contact electrodes (Ti/Au: 5 nm/90 nm). Electrical transport properties of the samples were measured from room temperature to 1.9 K with magnetic fields up to 9 T in a Physical Property Measurement System (Quantum Design, DynaCool).

Supporting Information

Supporting Information is available from the Wiley Online Library or from the author.

Acknowledgements

We thank Dr. Yu Zhou and Haifeng Yan for the beneficial discussions. We are also grateful to Dr. Alexei Barinov for his kind help and support during our beamtime at the spectramicroscopy beamline of Elettra synchrotron. This work was financially supported by the National Basic Research Program of China (Grants Nos. 2014CB932500, 2013CB932603, and 2012CB933004), the National Natural Science Foundation of China (Grants Nos. 21525310, 51520105003, 21173004, 51121091, 51522201, 11474006, and 11374019), National Program for Support of Top-Notch Young Professionals, and Beijing Municipal Science & Technology Commission (No. Z161100002116002). Part of this work was performed at the Stanford Nano Shared Facilities.

Received: July 7, 2016
Revised: July 27, 2016
Published online: August 26, 2016

[1] Y. Hori, K. Kikuchi, S. Suzuki, *Chem. Lett.* **1985**, *11*, 1695.
[2] A. A. Peterson, F. Abild-Pedersen, F. Studt, J. Rossmeisl, J. K. Norskov, *Energ. Environ. Sci.* **2010**, *3*, 1311.
[3] E. R. Ronan, S. D. Sudhoff, S. R. Glover, D. L. Galloway, *IEEE T Power Deliver* **2002**, *17*, 537.
[4] C. Iwakura, Y. Fukumoto, H. Inoue, S. Ohashi, S. Kobayashi, H. Tada, M. J. Abe, *Power Sources* **1997**, *68*, 301.
[5] P. Arora, R. E. White, M. J. Doyle, *Electrochem. Soc.* **1998**, *145*, 3647.
[6] K. Mase, K. Yoshimura, *Denki Kagaku* **1992**, *60*, 543.
[7] K. Fellner, P. F. Fuchs, G. Pinter, T. Antretter, T. Krivec, *Circuit World* **2014**, *40*, 53.
[8] V. C. Sethi, *Electron. Inf. Plann.* **1993**, *21*, 40.
[9] U. Stahlberg, H. Keife, *J. Mater. Process Tech.* **1993**, *37*, 157.
[10] X. S. Li, W. W. Cai, J. H. An, S. Kim, J. Nah, D. X. Yang, R. Piner, A. Velamakanni, I. Jung, E. Tutuc, S. K. Banerjee, L. Colombo, R. S. Ruoff, *Science* **2009**, *324*, 1312.
[11] S. Bae, H. Kim, Y. Lee, X. F. Xu, J. S. Park, Y. Zheng, J. Balakrishnan, T. Lei, H. R. Kim, Y. I. Song, Y. J. Kim, K. S. Kim, B. Ozyilmaz, J. H. Ahn, B. H. Hong, S. Iijima, *Nat. Nanotechnol.* **2010**, *5*, 574.
[12] K. Yan, L. Fu, H. L. Peng, Z. F Liu, *Acc. Chem. Res.* **2013**, *46*, 2263.
[13] T. Hesjedal, *Appl. Phys. Lett.* **2011**, *98*,133106.

[14] B. Deng, P. C. Hsu, G. C. Chen, B. N. Chandrashekar, L. Liao, Z. Ayitimuda, J. X. Wu, Y. F. Guo, L. Lin, Y. Zhou, M. Aisijiang, Q. Xie, Y. Cui, Z. F. Liu, H. L. Peng, *Nano Lett.* **2015**, *15*, 4206.
[15] J. D. Wood, S. W. Schmucker, A. S. Lyons, E. Pop, J. W. Lyding, *Nano Lett.* **2011**, *11*, 4547.
[16] B. Wang, H. R. Y. H. Zhang, Z. Y. Chen, Z. Jin, X. Y. Liu, L. Z. Hu, G. H. Yu, *Mater. Lett.* **2014**, *131*, 138.
[17] A. Ibrahim, S. Akhtar, M. Atieh, R. Karnik, T. Laoui, *Carbon* **2015**, *94*, 369.
[18] L. Lin, J. Y. Li, H. Y. Ren, A. L. Koh, N. Kang, H. L. Peng, H. Q. Xu, Z. F. Liu, *ACS Nano* **2016**, *10*, 2022.
[19] O. V. Yazyev, S. G. Louie, *Phys. Rev. B* **2010**, *81*,195420.
[20] O. V. Yazyev, S. G Louie, *Nat. Mater.* **2010**, *9*, 806.
[21] P. Y. Huang, C. S. Ruiz-Vargas, A. M. van der Zande, W. S. Whitney, M. P. Levendorf, J. W. Kevek, S. Garg, J. S. Alden, C. J. Hustedt, Y. Zhu, J. Park, P. L. McEuen, D. A. Muller, *Nature* **2011**, *469*, 389.
[22] Q. K. Yu, L. A. Jauregui, W. Wu, R. Colby, J. F. Tian, Z. H. Su, H. L. Cao, Z. H. Liu, D. Pandey, D. G. Wei, T. F. Chung, P. Peng, N. P. Guisinger, E. A. Stach, J. M. Bao, S. S. Pei, Y. P. Chen, *Nat. Mater.* **2011**, *10*, 443.
[23] T. Iwasaki, H. J. Park, M. Konuma, D. S. Lee, J. H. Smet, U. Starke, *Nano Lett.* **2011**, *11*, 79.
[24] J. H. Lee, E. K. Lee, W. J. Joo, Y. Jang, B. S. Kim, J. Y. Lim, S. H. Choi, S. J. Ahn, J. R. Ahn, M. H. Park, C. W. Yang, B. L. Choi, S. W. Hwang, D. Whang, *Science* **2014**, *344*, 286.
[25] V. L. Nguyen, B. G. Shin, D. L. Duong, S. T. Kim, D. Perello, Y. J. Lim, Q. H. Yuan, F. Ding, H. Y. Jeong, H. S. Shin, S. M. Lee, S. H. Chae, Q. A. Vu, S. H. Lee, Y. H. Lee, *Adv. Mater.* **2015**, *27*, 1376.
[26] T. R. Wu, X. F. Zhang, Q. H. Yuan, J. C. Xue, G. Y. Lu, Z. H. Liu, H. S. Wang, H. M. Wang, F. Ding, Q. K. Yu, X. M. Xie, M. H. Jiang, *Nat. Mater.* **2016**, *15*, 43.
[27] Y. F. Hao, M. S. Bharathi, L. Wang, Y. Y. Liu, H. Chen, S. Nie, X. H. Wang, H. Chou, C. Tan, B. Fallahazad, H. Ramanarayan, C. W. Magnuson, E. Tutuc, B. I. Yakobson, K. F. McCarty, Y. W. Zhang, P. Kim, J. Hone, L. Colombo, R. S. Ruoff, *Science* **2013**, *342*, 720.
[28] H. L. Zhou, W. J. Yu, L. X. Liu, R. Cheng, Y. Chen, X. Q. Huang, Y. Liu, Y. Wang, Y. Huang, X. F. Duan, *Nat. Commun.* **2013**, *4*, 2096.
[29] Z. Yan, J. Lin, Z. W. Peng, Z. Z. Sun, Y. Zhu, L. Li, C. S. Xiang, E. L. Samuel, C. Kittrell, J. M. Tour, *ACS Nano* **2012**, *6*, 9110.
[30] A. Mohsin, L. Liu, P. Z. Liu, W. Deng, I. N. Ivanov, G. L. Li, O. E. Dyck, G. Duscher, J. R. Dunlap, K. Xiao, G. Gu, *ACS Nano* **2013**, *7*, 8924.
[31] S. S. Chen, H. X. Ji, H. Chou, Q. Y. Li, H. Y. Li, J. W. Suk, R. Piner, L. Liao, W. W. Cai, R. S. Ruoff, *Adv. Mater.* **2013**, *25*, 2062.
[32] W. Guo, F. Jing, J. Xiao, C. Zhou, Y. Lin, S. Wang, *Adv. Mater.* **2016**, *28*, 3152.
[33] K. Xu, Z. H. Li, *J. Fluid Mech.* **2004**, *513*, 87.
[34] A. V. Kuznetsov, D. A. Nield, *Transport Porous Med.* **2006**, *65*, 505.
[35] S. Bhaviripudi, X. T. Jia, M. S. Dresselhaus, J. Kong, *Nano Lett.* **2010**, *10*, 4128.
[36] J. C. Meyer, A. K. Geim, M. I. Katsnelson, K. S. Novoselov, T. J. Booth, S. Roth, *Nature* **2007**, *446*, 60.
[37] A. C. Ferrari, J. C. Meyer, V. Scardaci, C. Casiraghi, M. Lazzeri, F. Mauri, S. Piscanec, D. Jiang, K. S. Novoselov, S. Roth, A. K. Geim, *Phys. Rev. Lett.* **2006**, *97*, 187401.
[38] P. Sutter, M. S. Hybertsen, J. T. Sadowski, E. Sutter, *Nano Lett.* **2009**, *9*, 2654.
[39] K. S. Novoselov, A. K. Geim, S. V. Morozov, D. Jiang, M. I. Katsnelson, I. V. Grigorieva, S. V. Dubonos, A. A. Firsov, *Nature* **2005**, *438*, 197.
[40] X. Y. Zhang, L. Wang, J. Xin, B. I. Yakobson, F. Ding, *J. Am. Chem. Soc.* **2014**, *136*, 3040.
[41] E. Meca, J. Lowengrub, H. Kim, C. Mattevi, V. B. Shenoy, *Nano Lett.* **2013**, *13*, 5692.
[42] J. F. Tian, H. L. Cao, W. Wu, Q. K. Yu, N. P. Guisinger, Y. P. Chen, *Nano Lett.* **2012**, *12*, 3893.
[43] Q. H. Yuan, B. I. Yakobson, F. Ding, *J. Phys. Chem. Lett.* **2014**, *5*, 3093.
[44] J. F. Gao, J. Yip, J. J. Zhao, B. I. Yakobson, F. Ding, *J. Am. Chem. Soc.* **2011**, *133*, 5009.